New Journal of Physics
The open access journal for physics

Melting of hexagonal skyrmion states in chiral magnets

M C Ambrose[1] **and R L Stamps**[2]

[1] School of Physics, The University of Western Australia, 35 Stirling Highway, Crawley 6009, Australia
[2] SUPA School of Physics and Astronomy, University of Glasgow, Glasgow G12 8QQ, UK
E-mail: ambrom01@student.uwa.edu.au and Robert.Stamps@glasgow.ac.uk

New Journal of Physics **15** (2013) 053003 (15pp)
Received 20 September 2012
Published 7 May 2013
Online at http://www.njp.org/
doi:10.1088/1367-2630/15/5/053003

Abstract. Skyrmions are spiral structures observed in thin films of certain magnetic materials (Uchida *et al* 2006 *Science* **311** 359–61). Of the phases allowed by the crystalline symmetries of these materials (Yi *et al* 2009 *Phys. Rev.* B **80** 054416), only the hexagonally packed phases (SC_h) have been observed. Here the melting of the SC_h phase is investigated using Monte Carlo simulations. In addition to the usual measure of skyrmion density, chiral charge, a morphological measure is considered. In doing so it is shown that the low-temperature reduction in chiral charge is associated with a change in skyrmion profiles rather than skyrmion destruction. At higher temperatures, the loss of six-fold symmetry is associated with the appearance of elongated skyrmions that disrupt the hexagonal packing.

Contents

1. Introduction

Following early work by Pauli, a variety of nonlinear sigma models were suggested as models for baryons [3–5]. One of the first soluble models was found by Skyrme who considered rotational variables [6], and the resultant unit field spiral solitons are referred to as skyrmions. Two-dimensional skyrmions appeared as the fundamental excitation from a spin-polarized two-dimensional electron gas. It was suggested that defects could localize skyrmions, giving rise to the fractional quantum Hall effect (QHE) [7–9]. Observations in GaAs quantum well systems using NMR [10] and magnetoabsorption spectroscopy [11] confirmed the presence of quasi-particles with charges consistent with theoretical predictions. More recently, measurements have been made in GaAs using NMR relaxation [12], spin wave absorption [13] and microwave absorption [14], which are consistent with the presence of a predicted skyrmion lattice [15]. Skyrmions were first proposed as a possible magnetic spin texture by Bogdanov and Hubert, who showed that Dzyaloshinskii–Morya exchange terms could lead to stabilization of skyrmion crystals in chiral magnets [16–18]. Recently, real space measurements of the two-dimensional analogue of these spiral structures have been made at low temperature in thin films of $Fe_{0.5}Co_{0.5}Si$ [1, 19] and close to room temperature in FeGe [20], along with the measurement of spin torque effects at very low current densities [21]; these measurements have ignited interest in skyrmions as a possible candidate for magnetic storage [22].

In two dimensions, skyrmions exist as a vortex structure modulated by a changing perpendicular component. Consider a field of unit length $\hat{s}(\vec{x})$ with $\vec{x}$ two dimensional and $\hat{s}(\vec{x})$ taking the usual polar representation[3]. Away from an isolated skyrmion, the field is described by the zenith angle $\theta = \pi$. Taking radial coordinates (ρ, ψ) for $\vec{x}$, a skyrmion can be described as a vortex in the azimuthal angle $\phi(\rho, \psi) = \psi - \pi/2$ modulated by a radial varying zenith angle $\theta(\rho, \psi) = \theta(\rho)$ such that $\theta(0) = 0$ and $\theta(R) = \pi$. An example of close-packed skyrmions projected into the plane is shown in figure 1(c), where gray (black) arrows indicate spins with the perpendicular component pointing up (down). For such an excitation to be stable, one requires a Hamiltonian with either fourth-order derivatives of the field [6] or terms lacking inversion symmetry [16]. Lack of inversion symmetry can be found in a variety of crystal

[3] The zenith measured with respect to the z direction perpendicular to the plane.

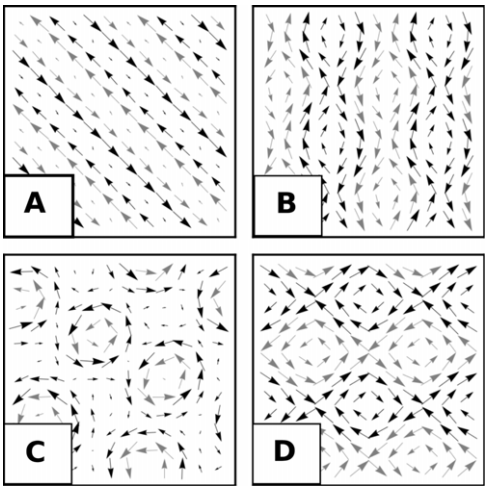

Figure 1. Projection of spins into the x–y plane; black arrows indicate that $s_i^z > 0$ while gray arrows indicate $s_i^z < 0$. (A) Helix state; (B) SC_1 skyrmion; (C) SC_h skyrmion; and (D) SC_2 skyrmion.

structures, in particular B20 crystal compounds with crystallographic point group 23,[4] in which Dzyaloshinskii–Morya coupling is present. Yi *et al* [2] calculated the $T = 0$ phase diagram as a function of external magnetic field and anisotropy for such a two-dimensional magnet using Monte-Carlo simulation.

Five different states were identified: the high-field saturated ferromagnetic phase, a helical state (figure 1(a)) and three chiral states. The chiral crystal states were labeled according to their rotational symmetries: SC_1 (figure 1(b)) has a two-fold rotational symmetry, SC_2 (figure 1(d)) shows a four-fold symmetry and SC_h (figure 1(c)) a six-fold symmetry[5]. In what follows, we restrict our attention to the SC_h-type skyrmions.

Analytically, the ground state properties of this two-dimensional case have been studied using a Landau–Ginzburg formalism [23]. The nature of the phase transition has already been investigated using combinatorics [24]. Here the authors considered the striped helical state structure shown in figure 1(a) as the ground state. In the presence of an external field perpendicular to the plane of the sample, one direction of perpendicular magnetization is favored. Since the stripe period is fixed by the ratio of Dzyaloshinskii–Morya and ferromagnetic exchange coupling, spins reverse inside stripes anti-aligned with the field, breaking the remaining anti-aligned areas into finite length stripes. Unlike the one-dimensional periodicity of the ground state (giving zero chiral density), the ends of the terminating stripes form a 'meron': a chiral half spiral. The skyrmion crystal state SC_h shown in figure 1(c) is the state with maximum possible meron density. By considering the merons as particles with chiral charge, a free energy can be written and a qualitatively correct B–T phase diagram produced. While the assumptions of this model are reasonable at low temperature, the possibility of skyrmion profiles changing with temperature cannot be described. One expects that as temperature is increased, thermal fluctuations will dominate and the particle description will no longer be valid.

[4] In Hermann Mauguin notation.

[5] This notation should not be confused with the notation of some authors in which skyrmion states are labeled as either SkX or SkG, referring to whether the system has formed a close-packed skyrmion crystal (SkX) or consists of spatially isolated skyrmions (SkG).

Current Monte Carlo simulations have focused on obtaining phase diagrams, with phases identified according to symmetry properties and chiral density [2, 19]. As a system with textured phase, close-packed skyrmions represent three types of order: a net chiral charge, a six-fold symmetry and a net magnetization. Here we use Monte Carlo simulations to investigate the melting of the SC_h phase, focusing on the mechanism through which these various orders are destroyed.

2. Theory and method

Typical magnetic skyrmions have diameters of hundreds of angstroms and so atomic scale modeling would be exceptionally demanding computationally. Instead we use a discretized version of the phenomenological continuum model proposed by Bak and Jensen [25], first introduced to explain observations of helical structure in MnSi [26–28] and FeGe [29]; the model has since been adapted to a discrete lattice by Yi *et al* [2] and we begin with their Hamiltonian. In two dimensions and in our notation, it reads

$$E = -J/2 \sum_{\langle i,j \rangle} \vec{s}_i \cdot \vec{s}_j - K/2 \sum_i ((\vec{s}_i \times (\vec{s}_{i+a\hat{x}} - \vec{s}_{i-a\hat{x}})) \cdot \hat{x} + (\vec{s}_i \times (\vec{s}_{i+a\hat{y}} - \vec{s}_{i-a\hat{y}})) \cdot \hat{y}) + \sum_i \vec{H} \cdot \vec{s}_i + A_1 \sum_i ((\vec{s}_i^{\,x})^4 + (\vec{s}_i^{\,y})^4 + (\vec{s}_i^{\,z})^4) + A_2 \sum_i (s_i^{\,x} s_{i+a\hat{x}}^{\,x} + s_i^{\,y} s_{i+a\hat{y}}^{\,y}). \quad (1)$$

For brevity we use single subscripts to represent locations on a two-dimensional square lattice with lattice constant a. The $\vec{s}_i$ are dimensionless spins at the vertices of this lattice representing the average magnetization of a small volume $V_i = a \times a \times t$ centered on vertex i, with t the thickness of the film. $\vec{s}_{i+a\hat{x}}$ and $\vec{s}_{i-a\hat{x}}$ represent the closest spins to $\vec{s}_i$ in the x direction (with analogous notation in the y direction) and $\sum_{\langle i,j \rangle}$ indicates a sum over all pairs of nearest neighbors. K is the strength of the Dzyaloshinskii–Morya exchange coupling, the sign of which determines the handedness of the skyrmions; J is the strength of the isotropic exchange coupling; H is the strength of the applied magnetic field and A_1 and A_2 are anisotropies. The ratio of exchange to Dzyaloshinskii–Morya strength determines the periodicity of the skyrmion lattice as $P = da$ where d is [2, 19]

$$d = 2\pi \left(\arctan \left(\frac{2\sqrt{2}K}{4J + A_2} \right) \right)^{-1}. \quad (2)$$

Since the computation time to complete a Monte Carlo step scales with the number of spins, simulating large systems is typically associated with long computation times. In order to decrease this computation time, GPU parallel programming is employed. The Hamiltonian includes only short-range interactions so a parallel checkerboard-type algorithm similar to those described by Weigel and Yavorskii [30, 31] is used.

2.1. Ground state packing

In order to relate the results of simulations performed on finite lattices to those expected for infinite systems, one exploits scaling relations between a set of universal scaling functions given as a function of an adjusted temperature $L^{1/\nu} T_c^{-1} (T - T_c)$. For modulated phases this involves selecting an appropriate order parameter and then selecting scaling sizes restricted to multiples

Table 1. Parameters used in the Monte Carlo simulation.

Parameter	Value
K/J	2.45
A_1/J	0.5
A_2/J	−0.25

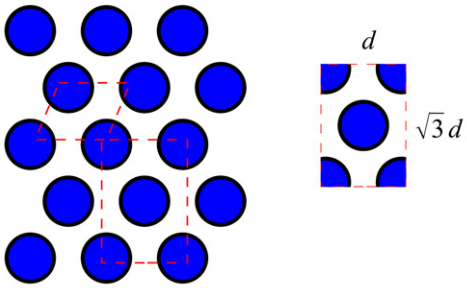

Figure 2. Left: unit cells that span a plane with hexagonal symmetry; right: the dimensions of a rectangular unit cell that can be used to tile a finite system with periodic boundary conditions.

of some appropriate unit cell. Such a procedure has been successful in calculating critical exponents for striped and anti-ferromagnetic Ising systems [32] (interestingly the resulting parameters do not belong to any known universality class). As a first step toward achieving a comparable framework for skyrmions, we focus here on a qualitative description of the dynamics and describe how various measures of the skyrmion phase evolve. We also comment on the challenge of defining a unit cell for phases with $P6$ symmetry.

For a hexagonal array with spacing d and axes in the $[1, 0]$ and $[1, \sqrt{3}]$ directions, one expects elements separated by vectors $\pm(d, 0)$, $\pm(d/2, \sqrt{3}/2)$ and $\pm(d/2, -\sqrt{3}/2)$ to have the same value. On a square lattice, $\pm(d/2, \sqrt{3}d/2)$ and $\pm(d/2, -\sqrt{3}d/2)$ are non-integer and hence do not correspond to lattice sites. In order to select a value for d that favors hexagonal packing, we select the value of d for which $\pm(d, 0)$, $\pm(d/2, \sqrt{3}/2)$ and $\pm(d/2, -\sqrt{3}/2)$ are as close to integer values as possible. Considering sizes less than ten (to keep computation times acceptable), the best choice is $d = 6$. This value has been considered in previous simulations [2, 19]. Parameters used are given in table 1, where dimensionless quantities are given by normalizing against J. In what follows, temperature and energy will be given as $\mathcal{T} = (k_B T)/J$ and energy as $\mathcal{E} = E/J$. The magnetic field is fixed at $H/J = 1.875$ to ensure that at $\mathcal{T} = 0$ the system forms close-packed skyrmions. With this choice of parameters, one lattice spacing in the discretized model represents between 3 and 15 nm.

Some care should be taken when choosing the finite dimension (L) of the spin lattice for these calculations. For skyrmions the ground state is periodic, consisting of hexagonally close-packed skyrmions; hence the repeated unit cell of the crystal lattice is not square. In order to tile a pattern with six-fold symmetry, one usually selects a unit cell that is a parallelogram defined by the vectors $v_1 = (d, 0)$ and $v_2 = (d/2, \sqrt{3}d/2)$, where d is the spacing between six-fold symmetry axes (in this case skyrmion cores). The resulting parallelogram is indicated in figure 2. This parallelogram unit cell is space filling and can be used to cover an infinite plane.

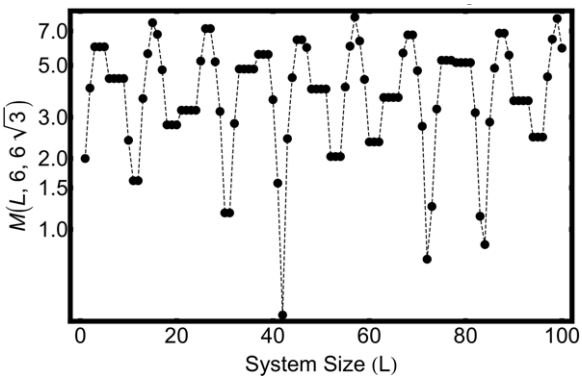

Figure 3. Log plot of $M(L, 6, 6\sqrt{3})$ showing the minimum at $L = 42$. This minimum corresponds to the tiling that best minimizes finite size effects introduced by periodic boundary conditions.

Our simulation uses a square lattice spanning a finite region with periodic boundary conditions. In order to tile a space with periodicity in the x and y directions, we select a rectangle to act as the unit cell, also shown in figure 2. This unit cell is then a rectangle with width $d_1 = d$ and height $d_2 = \sqrt{3}d$. The above parameters for which $d = 6$ correspond to a unit cell of dimensions 6×10.3923. If one picks a system size with periodic boundary conditions and length as multiples of d, the resultant state will be influenced in one direction by the forced periodicity. When deciding the system size, one should attempt to find a system size that is a multiple of d_1 and d_2. With d_2 irrational, this is not possible. Instead we consider the two lengths that define the unit cell $d_1 = 6$ and $d_2 = 6\sqrt{3}$. In order to measure the amount of mismatch between the system size L and the unit cell, we define a function

$$M(L, d_1, d_2) = \min(L - d_2\lfloor L/d_2 \rfloor, d_2 - L + d_2\lfloor L/d_2 \rfloor) + \min(L - d_1\lfloor L/d_1 \rfloor, d_1 - L + d_1\lfloor L/d_1 \rfloor), \quad (3)$$

where each term in equation (3) is a measure of how far L is from an exact multiple of d_1 or d_2. In the case of the hexagonal skyrmion lattice where d_2 is irrational and L is restricted to be an integer, the minima are not known *a priori*. In order to select a reasonable size, $M(L, 6, 6\sqrt{3})$ was calculated for $L \in [1, 100]$. As shown in figure 3, the minimum value is found to be $L = 42$.

2.2. Analysis

The close-packed skyrmion ground state consists of two types of order, a chiral charge associated with the creation of spiral structures and a long-range order associated with the hexagonal packing. In addition to the skyrmion crystal order, the system has a net magnetization in response to the applied magnetic field.

Two techniques are employed in order to measure the number of skyrmions in a state. The first is to consider the topological charge Q of a skyrmion, which is the sum of the local chiral charge over the area of a single skyrmion [24]. The charge density is the discretized form of the continuum expression

$$\chi = \frac{1}{4\pi} \int \mathrm{d}^2x \, \vec{s} \cdot (\partial_x \vec{s} \times \partial_y \vec{s}), \quad (4)$$

giving

$$\chi_i = \frac{1}{4\pi a^2}\vec{s}_i \cdot ((\vec{s}_{i+a\hat{x}} - \vec{s}_{i-a\hat{x}}) \times (\vec{s}_{i+a\hat{y}} - \vec{s}_{i-a\hat{y}})). \tag{5}$$

The chiral charge is then $\chi = N^{-1}\sum_i \chi_i$. We are aware of an earlier discretization of chiral charge, which we discuss in the appendix. In order to define the charge Q of a skyrmion, we calculate the total charge of the ground state and divide by the number of skyrmions. Assuming that the skyrmion charge is constant with changing $\mathcal{T}$ and that phase transition occurs via changing skyrmion density (i.e. destruction of skyrmions), one could calculate the number of skyrmions at any finite temperature by dividing the total charge by Q. This method of counting skyrmions assumes that the skyrmion charge remains constant (i.e. the skyrmion profile is not temperature dependent). In order to scrutinize this assumption, we define a second measure of skyrmion number that does not assume constant charge. Since the core of a skyrmion points against the applied magnetic field, one can binarize a state by applying $\Theta(1/2(\vec{s}_i \cdot \hat{z} + 1) - T_r)$ (Θ is the Heaviside Theta function), where T_r is some threshold between zero and one. In doing so one identifies spins with $\vec{s}_i \cdot \hat{z}$ anti-parallel to the magnetic field as skyrmion cores. One can then calculate the connected components of the resultant state. To do this the eight nearest and next-nearest neighbors to a given spin are considered connected if they are equal. Counting the total number of connected components gives a measure of the skyrmion number. This measure of skyrmion number assumes that skyrmion cores align anti-parallel to the applied field. While both orientations carry the same Dzyaloshinskii–Morya coupling energy, cores aligning with the field possess a higher Zeeman energy cost (since the core occupies less area than the outside of the skyrmion), so a state of close-packed skyrmions oriented with cores aligned with the field is not favored. The possibility of mixed cores (some parallel, some anti-parallel) has an energy cost due to exchange coupling at the boundary between skyrmions. For sufficiently strong two-site anisotropy, this can be overcome leading to the states shown in figures 1(b) and (d) [2]. The possibility of mixed cores may increase near the transition, especially in finite systems or near defects, but was not observed in the cases studied here. By comparing these two measures of skyrmion number, one can distinguish between reduction of topological charge due to skyrmion destruction and alteration of the skyrmion profile.

In order to examine the long-range order of a state, the Fourier transform $\vec{S}_k = \sum_j \vec{s}_j \exp(\mathrm{i}k \cdot j)$ is taken. When the system is close packed, $|\vec{S}_k|$ will have six satellite peaks corresponding to the hexagonal symmetry of the ground state.

3. Results

For each system size to be investigated, the ground state is first calculated by starting the system in a random configuration and then reducing the temperature to zero over 10^7 MC steps. The ground state for $L = 42$ is shown in figure 4 along with the intensity profile of the Fourier transform $|\vec{S}_k|$. By selecting the system size L to match the dimensions of the rectangular unit cell described above, it is possible to fit an integer number of unit cells into the square array. Here the Fourier transform shows a slight deviation from a perfectly hexagonal packing, which we discuss in section 4. For finite temperature results, the system is evaluated at a constant temperature starting from the ground state with the first 10^7 MC steps disregarded to allow the system to equilibrate. An ensemble of 100 states is calculated and 280 MC steps are taken between subsequent states to ensure that each state is selected independently. In figure 5 four

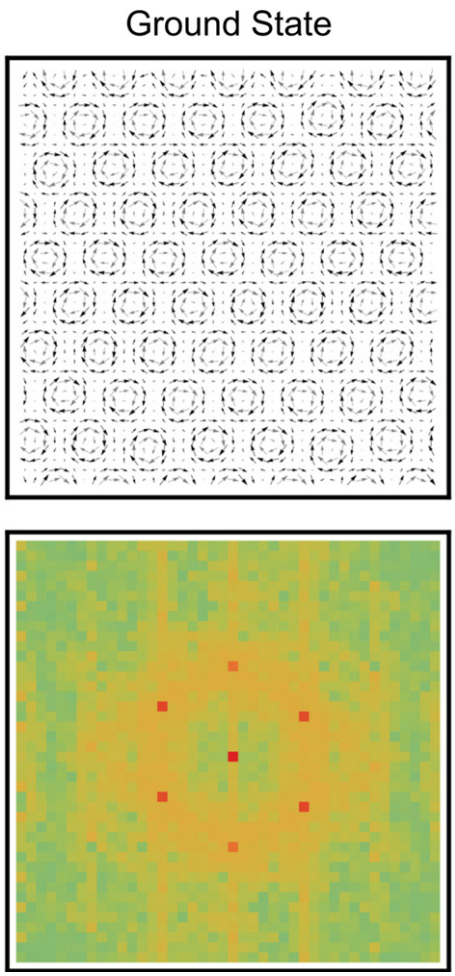

Figure 4. Ground state spin configuration (top) and intensity of the Fourier transform (bottom) showing peaks characteristic of the six-fold translational symmetry of the hexagonal lattice.

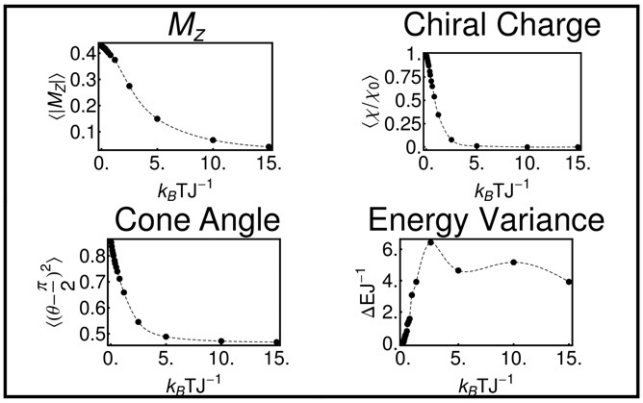

Figure 5. Clockwise from top left: perpendicular magnetization, chiral charge, cone angle and energy variance.

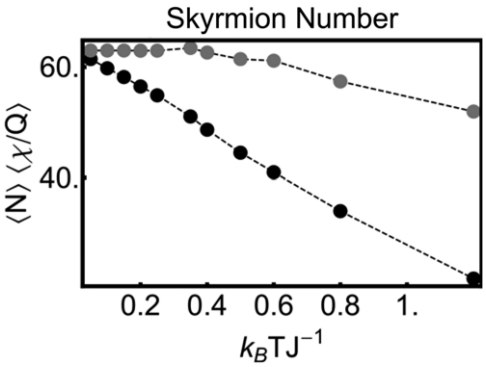

Figure 6. Two measures of skyrmion packing as a function of temperature: the connected reversed components (gray circles) and the ratio of total chiral charge to the charge of one skyrmion in the ground state $\langle\chi\rangle/Q$ (black circles).

order parameters of the system are shown: the magnetization $M_z = |N^{-1}\sum_i \vec{s}_i \cdot \hat{z}|$; the cone angle $(\theta_i - \pi/2)^2$; the chiral charge χ normalized against its ground state value; and the energy variance var($\mathcal{E}$). The persistence of the magnetic response at temperatures greater than those required for the destruction of chiral order is seen through the magnetization M_z and the cone angle. The loss of chiral structure occurs around $\mathcal{T} = 3$, but the elevated cone angle and magnetic order persist at approximately $\mathcal{T} = 8$. The energy variance is double peaked, indicating two broad transitions. At high temperatures, the entropy dominates and there is no order. Below $\mathcal{T} = 10$ there exists a region in which the cone angle increases from its high-temperature value giving rise to a non-zero magnetization. The external field ensures that as the temperature is decreased, the magnetization increases. The broad $\mathcal{T} = 10$ peak in the energy variance reflects the very gradual decay of magnetic response expected in the presence of an applied field; magnetic order is a single-site property and so it can persist at higher temperatures with a symmetry breaking field. Below approximately $\mathcal{T} = 2.5$, there is a transition into the skyrmion state characterized by the sharp increase in the strength of the chiral charge. Since the creation of skyrmions prevents the system reaching saturation, we note that the magnetization remains well below the saturation value.

3.1. Loss of six-fold order

In order to examine the loss of long-range order, we focus on the low-temperature regime. In figure 6 the skyrmion number is calculated using the total chiral charge and the method of counting cores described previously. While the chiral measure is reduced at all finite temperatures, the number of reversed regions remains constant below about $\mathcal{T} = 0.3$. This suggests that the initial loss of chiral charge is due to thermal distortion of the skyrmion profiles rather than destruction of the skyrmions themselves. In figure 7 an example state from ensembles at different temperatures is shown along with $|\vec{S}_k|$, between $\mathcal{T} = 0.1$ and 2.5. At $\mathcal{T} = 0.4$ the strong six-fold symmetry is compromised with peaks beginning to smear together. At $\mathcal{T} = 0.5$ the peaks have smeared into a circle, indicating that while a dominant length scale still exists six-fold translational symmetry is lost. At this temperature one can simultaneously observe the appearance of elongated regions of reversed magnetization. As temperature is further increased, any order in the perpendicular components of $\vec{s}_i$ is destroyed. An enlarged example of a state at $\mathcal{T} = 0.5$ is shown in figure 8. In addition to the perpendicular magnetic order, in-plane

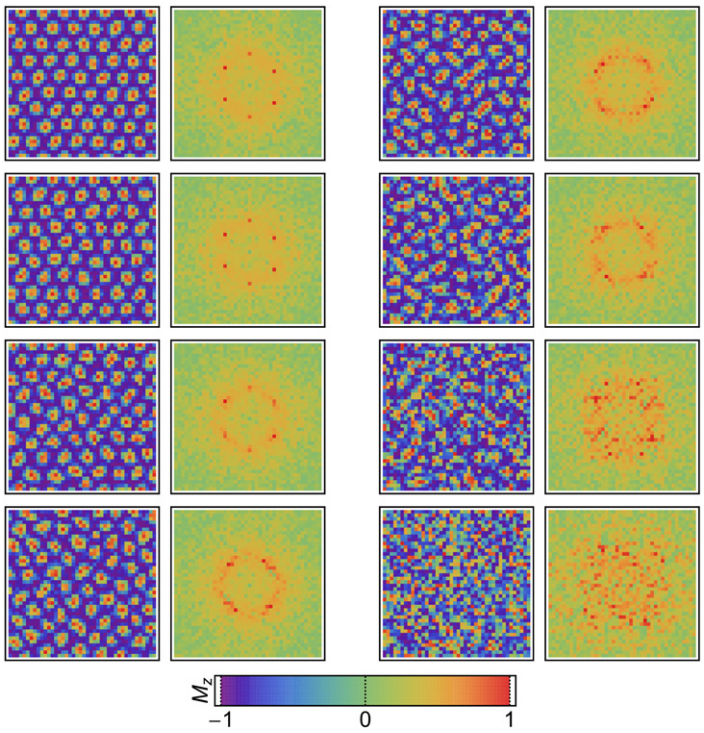

Figure 7. Perpendicular components of $\vec{s}_i$ and Fourier intensity $|\vec{S}_k|$ near the phase transition. Since the central ($k = 0$) Fourier peak is significantly larger than the satellite peaks at finite temperature, it is removed to give contrast. The Fourier plots then have their colors scaled with green representing zeros and red representing the maximum value. Perpendicular components of $\vec{s}_i$ are colored according to the legend above. Left column from top: $\mathcal{T} = 0.1$, 0.2, 0.35 and 0.4; right column from top: $\mathcal{T} = 0.5$, 0.8, 1.2 and 2.5.

magnetic order is shown as arrows. In addition to disrupting the close packing of skyrmions, these extended structures also reduce the chiral density described in equation (5). To illustrate this, in figure 9 the longest of extended regions shown in figure 8 is replotted with information about perpendicular order omitted. Color is used to indicate areas of highest chiral density, blue represents areas of low density and red indicates areas of high density. Here only the ends of the structure contribute significantly.

4. Effects of distorted packing

While the difficulty associated with finite size effects was minimized by considering the dimensions of the ground state unit cells, it is not possible to achieve perfect hexagonal packing. In addition, the presence of the low-temperature (below $\mathcal{T} = 0.3$) distortion of the skyrmion profile and the appearance of elongated regions might indicate a change of the dominant length scale. In order to investigate the effects of imperfect packing, several other comparable system sizes were investigated for $\mathcal{T} = 0.2$ and 0.4. The resulting energies are given in table 2, where it is seen that at finite temperature the change in energy due to finite size effects is not significant.

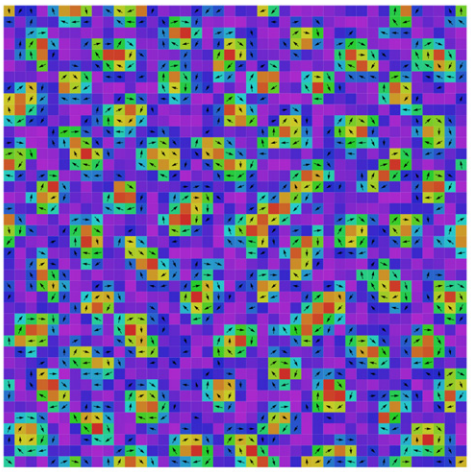

Figure 8. An example of the elongated structures associated with the destruction of long-range order at $\mathcal{T} = 0.5$. Here the perpendicular components of the spins are represented by color as in figure 7; in addition, for spins parallel to the plane their direction is indicated with arrows.

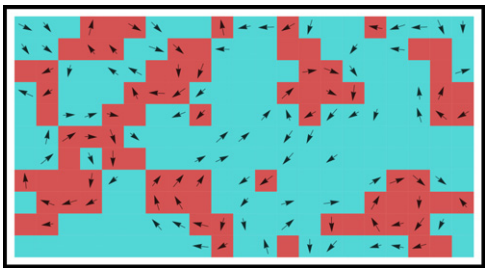

Figure 9. An example of the elongated structures associated with the destruction of long-range order at $\mathcal{T} = 0.5$. Spins parallel to the plane have their direction indicated with arrows. Areas of high chiral density are indicated in red.

Table 2. Ensemble energies for $\langle \mathcal{E} \rangle$ at $\mathcal{T} = 0.2$ and 0.4.

L	$\langle \mathcal{E} \rangle (\mathcal{T} = 0.2)$	$\langle \mathcal{E} \rangle (\mathcal{T} = 0.4)$
39	−2.318 98	−2.144 08
42	−2.320 90	−2.140 87
45	−2.324 48	−2.138 14
48	−2.319 05	−2.138 81

$\langle |\vec{S}_k| \rangle$ was also calculated and the results are shown in figure 10. If the spacing between skyrmions or skyrmion packing was to change with temperature, one expects that a small increase in system size might alter the stability of six-fold ordering near the phase transition. Systems with size L equal to 45 or 48 show the same general trend in which the six-fold order is destroyed leaving peaks in the [1, 1] and [−1, 1] directions. For $L = 39$ the system does not form six-fold packing. This strong size effect emphasizes the importance of a judicious choice of

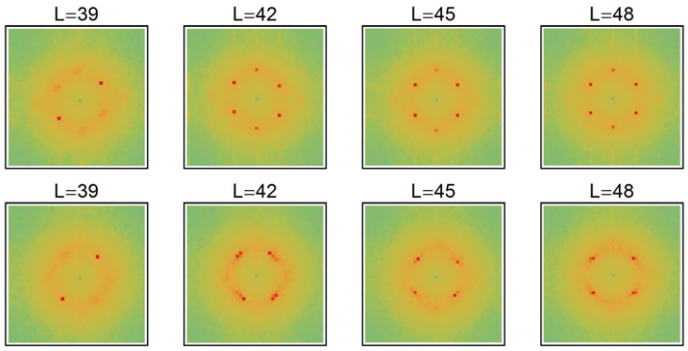

Figure 10. $\langle|\vec{S}_k|\rangle$ as a function of size for $\mathcal{T} = 0.2$ (top) and $\mathcal{T} = 0.4$ (bottom). The plots are colored as in figure 7.

system size. Even in the presence of this strong size effect, $L = 39$ (and the two larger systems) displays the same general morphological properties, a temperature-driven reduction in skyrmion density associated with the appearance of elongated structures. While the lack of atomic scale modeling means that our theory is likely not valid exactly at the phase transition, the qualitative description of the phase description given here is valid.

5. Conclusions and comments

We have shown that since the chiral density changes smoothly over a large temperature range, it does not capture all of the information about the melting process from the SC_h phase in chiral magnets. The Fourier intensity and the reversed connected components of the system reveal a low-temperature reduction in the chiral charge due to thermal distortion of the skyrmion profiles. At higher temperatures there is a sharp loss of six-fold order associated with the creation of elongated structures that disrupt ordering. Only the ends of these structures contribute to the chiral charge, further reducing the chiral density. In addition, it has been shown that the nature of hexagonal close packing means that while any choice of simulation size will introduce finite size effects, a judicious choice of system size can help alleviate these effects.

Here the authors have limited the scope of investigation to a single choice of applied field; however, the techniques presented might offer insight for a wide variety of fields. Specifically, there is the possibility that at higher fields the relative strength $\sum_i \vec{H} \cdot \vec{s}_i$ might suppress the creation of extended regions of reversed magnetization. There exists also the possibility of analyzing the zero-field ground state as stripes of alternating connected regions of perpendicular spins pointing in the positive and negative z direction, represented as $\Theta(1/2(\pm\vec{s}_i \cdot \hat{z} + 1) - T_r)$. Similarly the SC_1 and SC_2 phases might be analyzed as checkerboard alternating cores.

As discussed in section 2.1, parameters were chosen to provide skyrmion diameters of the order of tens of nanometers in order to correspond to observations of skyrmion orderings made on FeCoSi (∼90 nm [1]) and FeGe (∼70 nm [29]). Real space measurements of chiral structures are performed using Lorentz TEM and quantitative phase information is extracted by inverting the transport of intensity equation [1, 19, 33]. In this case calculating the skyrmion density is analogous to the measure of counting cores discussed in section 2.2. Chiral ordering is also associated with the anomalous QHE [2, 34, 35] and so measurements of skyrmion density based on Hall conductivity are likely to measure the chiral charge, which we have discussed in

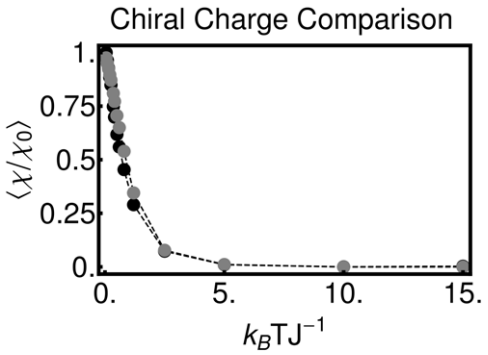

Figure A.1. Comparison of the two discretization schemes for chiral charge.

figures 5 and 6. The differing densities calculated from skyrmion counting and the chiral charge may have important implications for the interpretation of QHE measurements on quasi-two-dimensional skyrmion forming systems.

Small skyrmion-like structures can exist close to the atomic scale (see e.g. [36]); however, these are not described by our model. Instead, we model systems that support skyrmion textures on the length scales discussed above. These have dimensions of the order of tens of nanometers and it is therefore unlikely that isolated atomic level defects will have significant effects. In real systems the influence of the underlying lattice seems to be small (see e.g. [37]). We cannot rule out the possibility of pinning of skyrmion cores, however, which may be well localized. Defects that lead to pinning could also break rotational symmetry. Rotational symmetry breaking terms are included in our Hamiltonian (A_1 and A_2 anisotropy terms in equation (1)). Numerically, these terms are kept small in order to avoid the unphysical SC_2 phase described in the introduction.

Acknowledgments

The authors acknowledge funding from the Australian Government Department of Innovation, Industry, Science and Research, the Australian Research Council, the University of Western Australia and the Scottish Universities Physics Alliance.

Appendix. Comparison of chiral discretization

In our work here we have used a simple lattice derivative to evaluate the continuum expression given in equation (4). Berg and Lüscher [38] have defined an alternative discretization, in which the expression is given for a new set of sites equidistant from the original lattice vertices. Denoting sites on this new lattice $i*$ the definition is

$$\chi_{i*} = \frac{1}{4\pi}\left(\mathrm{sign}(\vec{s}_1 \cdot (\vec{s}_2 \times \vec{s}_3))A(\vec{s}_1, \vec{s}_2, \vec{s}_3) - \mathrm{sign}(\vec{s}_1 \cdot (\vec{s}_3 \times \vec{s}_4))A(\vec{s}_1, \vec{s}_3, \vec{s}_4)\right), \tag{A.1}$$

where $\vec{s}_1, \vec{s}_2, \vec{s}_3$ and $\vec{s}_4$ are the four spins adjacent to $i*$ (in canonical order) and $A(\vec{s}_1, \vec{s}_2, \vec{s}_3)$ is the area of the spherical triangle defined by its three arguments. In figure A.1 we show the results of calculating the chiral charge using the expressions in equations (5) and (A.1) normalized against

their ground state values. Here we observe that both discretization schemes give qualitatively the same results.

References

[1] Uchida M, Onose Y, Matsui Y and Tokura Y 2006 Real-space observation of helical spin order *Science* **311** 359–61

[2] Yi S D, Onoda S, Nagaosa N and Han J H 2009 Skyrmions and anomalous Hall effect in a Dzyaloshinskii–Moriya spiral magnet *Phys. Rev.* B **80** 054416

[3] Pauli W 1948 *Meson Theory of Nuclear Forces* (New York: Interscience)

[4] Skyrme T H R 1958 A nonlinear theory of strong interactions *Proc. R. Soc. Lond.* A **247** 260–78

[5] Skyrme T H R 1959 A unified model of k- and π-mesons *Proc. R. Soc. Lond.* A **252** 236–45

[6] Skyrme T H R 1961 A nonlinear field theory *Proc. R. Soc. Lond.* A **260** 127–38

[7] Zhang S C, Hansson T H and Kivelson S 1989 Effective-field-theory model for the fractional quantum Hall effect *Phys. Rev. Lett.* **62** 82–5

[8] Lee D-H and Kane C L 1990 Boson-vortex-skyrmion duality, spin-singlet fractional quantum Hall effect and spin-1/2 anyon superconductivity *Phys. Rev. Lett.* **64** 1313–7

[9] Sondhi S L, Karlhede A, Kivelson S A and Rezayi E H 1993 Skyrmions and the crossover from the integer to fractional quantum Hall effect at small Zeeman energies *Phys. Rev.* B **47** 16419–26

[10] Barrett S E, Dabbagh G, Pfeiffer L N, West K W and Tycko R 1995 Optically pumped NMR evidence for finite-size skyrmions in GaAs quantum wells near Landau level filling $\nu = 1$ *Phys. Rev. Lett.* **74** 5112–5

[11] Aifer E H, Goldberg B B and Broido D A 1996 Evidence of skyrmion excitations about $\nu = 1$ in n-modulation-doped single quantum wells by interband optical transmission *Phys. Rev. Lett.* **76** 680–3

[12] Gervais G, Stormer H L, Tsui D C, Kuhns P L, Moulton W G, Reyes A P, Pfeiffer L N, Baldwin K W and West K W 2005 Evidence for skyrmion crystallization from NMR relaxation experiments *Phys. Rev. Lett.* **94** 196803

[13] Gallais Y, Yan J, Pinczuk A, Pfeiffer L N and West K W 2008 Soft spin wave near $\nu = 1$: evidence for a magnetic instability in skyrmion systems *Phys. Rev. Lett.* **100** 086806

[14] Zhu H, Sambandamurthy G, Chen Y P, Jiang P, Engel L W, Tsui D C, Pfeiffer L N and West K W 2010 Pinning-mode resonance of a skyrme crystal near Landau-level filling factor $\nu = 1$ *Phys. Rev. Lett.* **104** 226801

[15] Brey L, Fertig H A, Côté R and MacDonald A H 1995 Skyrme crystal in a two-dimensional electron gas *Phys. Rev. Lett.* **75** 2562–5

[16] Bogdanov A and Hubert A 1994 Thermodynamically stable magnetic vortex states in magnetic crystals *J. Magn. Magn. Mater.* **138** 255–69

[17] Butenko A B, Leonov A A, Rößler U K and Bogdanov A N 2010 Stabilization of skyrmion textures by uniaxial distortions in noncentrosymmetric cubic helimagnets *Phys. Rev.* B **82** 052403

[18] Rössler U K, Bogdanov A N and Pfleidere C 2006 Spontaneous skyrmion ground states in magnetic metals *Nature* **442** 797–801

[19] Yu X Z, Onose Y, Kanazawa N, Park J H, Han J H, Matsui Y, Nagaosa N and Tokura Y 2010 Real-space observation of a two-dimensional skyrmion crystal *Nature Lett.* **465** 901–4

[20] Yu X Z, Kanazawa N, Onose Y, Kimoto K, Zhang W Z, Ishiwata S, Matsui Y and Tokura Y 2011 Near room-temperature formation of a skyrmion crystal in thin-films of the helimagnet FeGe *Nature Mater.* **10** 106–9

[21] Jonietz F *et al* 2010 Spin transfer torques in MnSi at ultralow current densities *Science* **330** 1648–51

[22] Kiselev N S, Bogdanov A N, Schäfer R and Rössler U K 2011 Chiral skyrmions in thin magnetic films: new objects for magnetic storage technologies? *J. Phys. D: Appl. Phys.* **44** 392001

[23] Han J H, Zang J, Yang Z, Park J-H and Nagaosa N 2010 Skyrmion lattice in a two-dimensional chiral magnet *Phys. Rev.* B **82** 094429

[24] Ezawa M 2011 Compact merons and skyrmions in thin chiral magnetic films *Phys. Rev.* B **83** 100408

[25] Bak P and Jensen M H 1980 Theory of helical magnetic structures and phase transitions in MnSi and FeGe *J. Phys. C: Solid State Phys.* **13** L881
[26] Ishikawa Y, Komatsubara T and Bloch D 1977 Magnetic phase diagram of MnSi *Physica* B + C **86–88** (Part 1) 401–3
[27] Ishikawa Y, Tajima K, Bloch D and Roth M 1976 Helical spin structure in manganese silicide MnSi *Solid State Commun.* **19** 525–8
[28] Kusaka S, Yamamoto K, Komatsubara T and Ishikawa Y 1976 Ultrasonic study of magnetic phase diagram of MnSi *Solid State Commun.* **20** 925–7
[29] Ludgren L, Beckman O, Attia V, Bhattacheriee S P and Richardson M 1970 Helical spin arrangement in cubic FeGe *Phys. Scr.* **1** 69
[30] Weigel M and Yavorskii T 2011 GPU accelerated Monte Carlo simulations of lattice spin models *CSP2011: Proc. 24th Workshop on Computer Simulation Studies in Condensed Matter Physics; Phys. Procedia* **15** 92–6
[31] Weigel M 2011 Simulating spin models on GPU *Comput. Phys. Commun.* **182** 1833–6
[32] Rastelli E, Regina S and Tassi A 2006 Phase transitions in a square Ising model with exchange and dipole interactions *Phys. Rev.* B **73** 144418
[33] Teague M R 1983 Deterministic phase retrieval: a Green's function solution *J. Opt. Soc. Am.* **73** 1434–41
[34] Onose Y, Takeshita N, Terakura C, Takagi H and Tokura Y 2005 Doping dependence of transport properties in $Fe_{1-x}Co_xSi$ *Phys. Rev.* B **72** 224431
[35] Neubauer A, Pfleiderer C, Binz B, Rosch A, Ritz R, Niklowitz P G and Böni P 2009 Topological Hall effect in the *a* phase of MnSi *Phys. Rev. Lett.* **102** 186602
[36] Heinze S, von Bergmann K, Menzel M, Brede J, André Kubetzka, Roland Wiesendanger, Bihlmayer G and Blügel S 2010 Spontaneous atomic-scale magnetic skyrmion lattice in two dimensions *Nature Phys.* **7** 713–8
[37] Mühlbauer S, Binz B, Jonietz F, Pfleiderer C, Rosch A, Neubauer A, Georgii R and Böni P 2009 Skyrmion lattice in a chiral magnet *Science* **323** 915–9
[38] Berg B and Lüscher M 1981 Definition and statistical distributions of a topological number in the lattice o(3) σ-model *Nucl. Phys.* B **190** 412–24